THE JOURNAL OF PHYSICAL CHEMISTRY A
A JOURNAL OF THE AMERICAN CHEMICAL SOCIETY

pubs.acs.org/JPCA

Article

Thermodynamic Analysis of Spin Crossover in Molecules and Solid State Materials with pySCO

Angel Albavera-Mata*

Cite This: J. Phys. Chem. A 2025, 129, 11032−11040

Read Online

ACCESS | Metrics & More | Article Recommendations

ABSTRACT: The study of spin-crossover phenomena in metal complexes is of significant importance in chemistry and materials science, with implications for both theoretical advancements and practical applications. Commonly, the analysis of electronic structure outputs in this domain involves labor-intensive ad hoc scripting that lacks standardization and transferability. The pySCO library here is presented to overcome these challenges. It is designed to automate and simplify thermodynamic analyses for this family of metal complexes, offering seamless integration with popular electronic structure codes. This work features a detailed case study on an Fe(II) metal complex to highlight the robust capabilities offered by the library and provide insights into the spin transition regimes for this material.

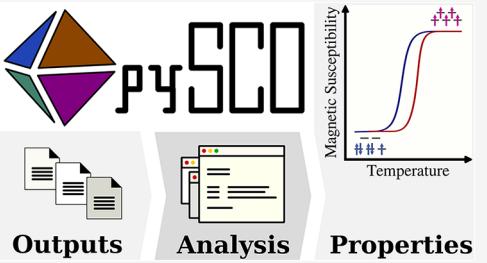

INTRODUCTION

Several molecular aggregates,[1−4] solutions,[5−7] or adsorbates[8−12] of coordination complexes with $3d^4$ to $3d^7$ metal cores may undergo spin-crossover transitions if the average crystal field parameter, 10 Dq, competes in magnitude with the electron pairing energy for the d-electrons.[13−16] This makes possible the existence of two ground states, which are populated or not, depending upon the crystal field strength. As a result, small external perturbations switch the metal complex to a low- or high-spin state.[17−20] These families of coordination adducts have been studied experimentally for nearly a century. The first report dates to the works of Polanyi,[21] and of Cambi and Szegö[22], and pioneering descriptions of Fe(II) spin transitions were given by Baker and Bobonich,[23] and by König and Madeja.[24] However, the development of theoretical models pursuing description of the phenomenon fell behind by nearly four decades, with the earliest work by Wajnflasz.[25,26]

It could be argued that a reason that hampered early developments of thermodynamic and microscopic models is, in part, that prediction of spin-conversion curves from simple modeling considerations poses a major challenge.[27−29] Given the relatively small energy interval for the spin gap, subtle changes to the composition of the ligands result in different transition profiles,[30−36] emergence of polymorphs,[37,38] or suppression of the spin conversion.[39] The resulting variations to the intra- and intermolecular cooperative interactions thus affect noticeably the spin equilibrium.

From the perspective of practical computational efforts, on the other hand, the need to facilitate efficient high-throughput analyses is becoming progressively more relevant for large-scale data curation of spin crossover candidates. These analyses allow one to model, and eventually understand, how different chemical functional groups influence the physical chemical properties for these materials. Common electronic structure codes like Gaussian,[40] NWChem,[41] Orca,[42] Vasp,[43] Quantum Espresso,[44] among others, offer parallelization advantages to achieve that purpose. However, post-treatment of output data most often still is done with ad hoc scripts crafted individually by different research groups. Such scripts are not readily available to the public, transferable between different electronic structure codes, easily reproducible nor, typically, have they been validated or cross-checked.

In this work, the problem is addressed by introducing the development of pySCO, a python library for automated scalable workflows with minimum user input requirements. Its use is showcased on an Fe(II) metal complex for the determination of the spin-crossover energy, transition temperature, thermal evolution of the magnetic susceptibility, and diverse analyses of the Gibbs free energy with the inclusion of a phenomenological interaction parameter.

Thermodynamic Fundamentals in the Library. The spin switching phenomenon and its diverse conversion behaviors may be treated theoretically with several models.[25−29,45−53] Among them, the basis for the regular solution model[54,55] consists of assuming that the spin state mixture for a given molecular aggregate is distributed statistically and forms a regular solution. For a given material at constant pressure, the

Received: August 21, 2025
Revised: October 16, 2025
Accepted: November 10, 2025
Published: November 14, 2025

https://doi.org/10.1021/acs.jpca.5c05841
J. Phys. Chem. A 2025, 129, 11032−11040

conversion from low to high spin is a thermal equilibrium between the spin configurations. The state function therefore is the Gibbs free energy $G = H - TS$, where H and S label the enthalpy and entropy for the system, respectively. Here, the largest contribution to G is the internal electronic energy for the low- and high-spin states, where a spin conversion energy no larger than 10 kJ mol^{-1} typically is expected for the spin crossover in molecules and materials.

The total electronic energy for each spin state is readily available from electronic structure computations. From those, the energy ΔE_{HL} for the spin crossover conversion

$$\Delta E_{HL} = E_{HS} - E_{LS} \tag{1}$$

is calculated from the total energy difference between the high- (HS) and low-spin (LS) states, E_{HS} and E_{LS}, respectively. It is important to clarify that ΔE_{HL} may also be found in the literature as $\Delta E_{sco} = \Delta E_{HL} + \Delta E_{zpe}$, that includes the zero-point vibrational energy difference ΔE_{zpe}.

As measured, the spin crossover is a cooperative behavior in a bulk molecular crystal. From that perspective, it is legitimate to consider a set of N weakly interacting molecules of which N_{HS} are in the high-spin state at temperature T. Therefore, the relative high-spin fraction is $n_{HS} = N_{HS}/N$, in terms of which the Gibbs free energy of an ideal solution model that includes the Gibbs free energy of the individual molecular spin states is

$$G = n_{HS}G_{HS} + (1 - n_{HS})G_{LS} - TS_{mix} \tag{2}$$

on the assumption that the intermolecular coupling has negligible dependence on those spin states, and that the ideal entropy of mixing, S_{mix}, in the thermodynamic limit is

$$S_{mix} = -k_B N_A(n_{HS}\ln[n_{HS}] + (1 - n_{HS})\ln[1 - n_{HS}]) \tag{3}$$

where N_A and k_B are Avogadro's number and Boltzmann's constant, respectively.

The equilibrium condition thus is obtained by minimizing G and calculating the associated maximum spin conversion

$$\left(\frac{\partial G}{\partial n_{HS}}\right)_{T,P} = 0 \tag{4}$$

Hence, the thermal evolution of n_{HS} is

$$T = \frac{\Delta H}{k_B N_A \ln[(1 - n_{HS})/n_{HS}] + \Delta S} \tag{5}$$

with the extremum

$$T_{1/2} = \left.\frac{\Delta H}{\Delta S}\right|_{n_{HS}=1/2} \tag{6}$$

being the transition temperature that corresponds to that which is reported experimentally. Notice from eq 5 that the equilibrium is defined by $n_{HS} = 1/2$, an equal population of low- and high-spin states, and that such equilibrium is reached at $T_{1/2}$ as defined by eq 6. Both ΔE_{HL}, and $T_{1/2}$ from eqs 1 and 6, respectively, can be computed with the pySCO library.

To deepen our analysis to the microscopic picture of the spin conversion phenomenon, next we focus attention on the enthalpy and entropy differences in eq 5, ΔH and ΔS, respectively. These are expressed in terms of the thermal expansion $P\,\Delta V$, as well as the electronic, vibrational, translational, and rotational contributions

$$\Delta H = \Delta E_{HL} + \Delta E_{vib} + \Delta E_{tra} + \Delta E_{rot} + P\Delta V \tag{7}$$

$$\Delta S = \Delta S_{ele} + \Delta S_{vib} + \Delta S_{tra} + \Delta S_{rot} \tag{8}$$

These are obtained by means of the vibrational factor $\theta_{vib,i} = h\nu_i/k_B$, that is computed from the set of harmonic vibrational frequencies $\{\nu_i\}$ for each spin state through the equations[56,57]

$$\Delta E_{vib} = k_B N_A \sum_{i\in HS}\left(\frac{\theta_{vib,i}}{2} + \frac{\theta_{vib,i}}{e^{\theta_{vib,i}/T} - 1}\right) - k_B N_A \sum_{i\in LS}\left(\frac{\theta_{vib,i}}{2} + \frac{\theta_{vib,i}}{e^{\theta_{vib,i}/T} - 1}\right) \tag{9}$$

$$\Delta S_{vib} = k_B N_A \sum_{i\in HS}\left(\frac{\theta_{vib,i}/T}{e^{\theta_{vib,i}/T} - 1} - \ln[1 - e^{\theta_{vib,i}/T}]\right) - k_B N_A \sum_{i\in LS}\left(\frac{\theta_{vib,i}/T}{e^{\theta_{vib,i}/T} - 1} - \ln[1 - e^{\theta_{vib,i}/T}]\right) \tag{10}$$

In addition, the change in the electronic entropy $\Delta S_{ele} = \Delta S_{spin} + \Delta S_{orb} + \Delta S_{Fermi}$, is given by three contributions, namely, $\Delta S_{spin} = k_B N_A \ln[(1 + 2S_{HS})/(1 + 2S_{LS})]$ that is associated with the change in the total spin S during the spin conversion, and the analogous expression for the entropy variation ΔS_{orb} due to orbital angular momentum L.[58] The Fermi entropy difference, ΔS_{Fermi}, on the other hand, depends on the Fermi distribution $f(\varepsilon) = 1/(1 + e^{\theta_{Fermi}/T})$, with $\theta_{Fermi} = (\varepsilon - \varepsilon_{Fermi})/k_B$, where ε and ε_{Fermi} are the single-particle energy state and Fermi energy, respectively, for each spin state, so that

$$\Delta S_{Fermi} = -k_B N_A \int n(\varepsilon)(f(\varepsilon)\ln[f(\varepsilon)] + (1 - f(\varepsilon))\ln[1 - f(\varepsilon)])d\varepsilon\Big|_{\{\varepsilon\}\in HS} + k_B N_A \int n(\varepsilon)(f(\varepsilon)\ln[f(\varepsilon)] + (1 - f(\varepsilon))\ln[1 - f(\varepsilon)])d\varepsilon\Big|_{\{\varepsilon\}\in LS} \tag{11}$$

where $n(\varepsilon)$ is the electronic density of states.[59] It is worth noting that because the spin-switching metal complexes have a well-defined gap, ΔS_{Fermi} is expected to contribute little if at all to the computed $T_{1/2}$.

The changes for the translational contributions to the energy and entropy, E_{tra} and S_{tra}, and the rotational energy E_{rot} either cancel or are sufficiently small that often they are neglected. Their expressions are[56,57]

$$E_{tra} = \frac{3}{2}k_B N_A T \tag{12}$$

$$S_{tra} = k_B N_A\left(\ln\left[\frac{k_B T}{P}\left(\frac{2\pi m}{h^2}k_B T\right)^{3/2}\right] + \frac{5}{2}\right) \tag{13}$$

$$E_{rot} = k_B N_A T \tag{14}$$

with h and m being the Planck constant and mass of the system, respectively.

The rotational contribution to the entropy, ΔS_{rot}, on the other hand, is given by the expression

https://doi.org/10.1021/acs.jpca.5c05841
J. Phys. Chem. A 2025, 129, 11032−11040

$$\Delta S_{\mathrm{rot}} = k_{\mathrm{B}} N_{\mathrm{A}} \ln\left[\frac{1}{\sigma_{\mathrm{r}}}\left(\frac{\pi T^3}{\theta_{\mathrm{r},x}\theta_{\mathrm{r},y}\theta_{\mathrm{r},x}}\right)^{1/2}\right]_{\{\sigma_{\mathrm{r}},\theta_{\mathrm{r}}\}\in\mathrm{HS}} - k_{\mathrm{B}} N_{\mathrm{A}} \ln\left[\frac{1}{\sigma_{\mathrm{r}}}\left(\frac{\pi T^3}{\theta_{\mathrm{r},x}\theta_{\mathrm{r},y}\theta_{\mathrm{r},x}}\right)^{1/2}\right]_{\{\sigma_{\mathrm{r}},\theta_{\mathrm{r}}\}\in\mathrm{LS}} \quad (15)$$

where σ_{r} is the rotational symmetry number, and the set $\{\theta_{\mathrm{r}}\}$ corresponds to the rotational temperatures that depend on the moment of inertia.[56,57]

It is clear from eqs 5 through 15 that n_{HS} and T, share a nonlinear dependence. This means that we must evaluate eq 5 numerically to find $T_{1/2}$. For each choice of n_{HS} during the numerical procedure, one also must compute all temperature-dependent terms in ΔH and ΔS, while looping through the harmonic frequencies, $\{\nu\}$, in eqs 9 and 10, and single-particle energy states, $\{\varepsilon\}$, in eq 11 for both the low- and high-spin states. This is one of the main tasks of pySCO. It is handled automatically by the library without requiring user intervention.

We have discussed so far the basics of gradual spin conversions for weakly interacting molecules. Nonetheless, some highly cooperative materials with comparatively stronger intermolecular interaction exhibit rather abrupt spin switching. An energy barrier between the spin states hinders rapid thermal equilibration. This splits the heating, $T_{\uparrow}$, and cooling, $T_{\downarrow}$, transition temperatures into two distinct values separated by a finite hysteresis $\Delta T_{\uparrow\downarrow} = T_{\uparrow} - T_{\downarrow}$.

Slichter and Drickamer[60] proposed the addition of a nonlinear mean-field term independent of T to the regular solution model to parametrize that splitting in the form

$$G = (1 - n_{\mathrm{HS}})G_{\mathrm{LS}} + n_{\mathrm{HS}}G_{\mathrm{HS}} + \Gamma n_{\mathrm{HS}}(1 - n_{\mathrm{HS}}) - TS_{\mathrm{mix}} \quad (16)$$

That represents the simplest approximation to modeling intermolecular interactions by means of a second-order term, Γ, that is independent of n_{HS}. A more thorough discussion of other more sophisticated models is available in ref 27.

The coefficient Γ for this second-order contribution in eq 16 is known as the phenomenological interaction parameter and, as the name suggests, accounts for the cooperative intermolecular interactions. Analyzing the behavior of G during the spin transition, with both eqs 2 or 16, is possible in the pySCO library for different isothermal profiles.

At this point, it is important to highlight the usefulness of the sign of Γ, namely, $\Gamma < 0$ is indicative that the molecules in the crystal prefer to be surrounded by other molecules with opposite spin, whereas the converse $\Gamma > 0$ is characteristic of molecules with preference for being enclosed by others with the same spin.

Furthermore, the equilibrium condition for eq 16 is the same as in eq 4, but with the following expression for the thermal evolution of n_{HS}

$$T = \frac{\Delta H + \Gamma(1 - 2n_{\mathrm{HS}})}{k_{\mathrm{B}}N_{\mathrm{A}}\ln[(1 - n_{\mathrm{HS}})/n_{\mathrm{HS}}] + \Delta S} \quad (17)$$

Note that in this model, the hysteresis contribution vanishes for $n_{\mathrm{HS}} = 1/2$, and thus eq 17 reduces to eq 5 because the term $\Gamma(1 - 2\, n_{\mathrm{HS}}) = 0|_{n_{\mathrm{HS}} = 1/2}$.

Experimental determination of the interaction parameter usually is done with a nonlinear least-squares fit to eq 17 to get an estimation for ΔH, ΔS, and Γ. The former two relate to $T_{1/2}$ through eq 6. Bear in mind that first-principles calculation of Γ has proven difficult to date,[27,29,61−66] both because of the complicated physical processes subsumed in its mean field, and because its magnitude is substantially smaller than ΔE_{sco}, calculation of which itself is computationally challenging. This phenomenological parameter results from averaging the different energy contributions to the intermolecular interactions in a lattice and, in consequence, Γ may undergo sign flips during lattice relaxations of molecular crystals.[67,68]

To compute Γ with electronic structure methods, customarily one samples a series of different microscopic mixtures of low- and high-spin state configurations using supercells. For instance, a unit cell with four metal centers has $2^4 = 16$ possible distributions, namely, one for $n_{\mathrm{HS}} = 0$ with all four being low-spin, and the opposite for $n_{\mathrm{HS}} = 1$; four for $n_{\mathrm{HS}} = 1/4$ with only one high-spin molecule, and four $n_{\mathrm{HS}} = 3/4$ for the converse; and finally six configurations for $n_{\mathrm{HS}} = 1/2$ with an equal mixture of molecules in both spin states. The total number of possible distributions evidently becomes larger for progressively increasing supercells, but it may be reduced due to the presence of symmetry-related configurations. The results for these spin distributions then are used for fitting the interaction parameter.[69−74]

COMPUTATIONAL DETAILS

With the purpose of demonstrating the capabilities of the pySCO library, we focus attention on the homoleptic complex $[\mathrm{Fe}(t\mathrm{Bu}_2\mathrm{qsal})_2]$, with an average $T_{1/2} = 123$ K reported experimentally and characterized in ref 75. This metal complex is constituted by two *tert*-butyl substituents on one side of the adduct while leaving the other side free of steric hindrance. That, arguably, helps increase the volatility of the material and, at the same time, preserve the strong elastic coupling between the neighboring molecules in the crystal. As a result, the material exhibits a hysteresis $\Delta T_{\uparrow\downarrow} = 12$ K that is evidence of the strong cooperative behavior during the abrupt spin transition.

Though there is nothing in principle that compels the user to do the electronic structure calculations with some form of density functional approximation, such calculations are far and away the most common, hence they are the context for the ensuing discussion. Before proceeding with the details for $[\mathrm{Fe}(t\mathrm{Bu}_2\mathrm{qsal})_2]$, the reader should be aware that the choice of density functional approximation plays a crucial role in determining the quality of the results, as does the admixture of single-determinant exchange.[79−81] The same may be said for distinct choices of level of theory known for delivering qualitatively different trends, even for small spin-crossover archetypes.[82,83] This study used periodic boundary conditions with the VASP 6.3 code and the set of standard PBE potpaw.54 projector augmented wave potentials for Fe, O, N, C, and H that correspond to the valence electron configurations $3s^2\ 3p^6\ 3d^7\ 4s^1$, $2s^2\ 2p^4$, $2s^2\ 2p^3$, $2s^2\ 2p^2$, and $1s^1$, respectively.[43] For the sake of consistency, the PBE generalized gradient exchange-correlation density functional approximation with the Hubbard-U correction for the Fe(II) $3d$ orbitals also was selected.[84−87] The value $U = 2$ eV was fitted as shown in Figure 1 to reproduce as closely as possible the reported experimental transition temperature $T_{1/2}^{\mathrm{expt}} = 123$ K for $[\mathrm{Fe}(t\mathrm{Bu}_2\mathrm{qsal})_2]$.[75] Specifically, each filled dot shown in Figure 1 was obtained by doing a cell and atomic coordinate optimization for the low- and high-spin states for each of the

https://doi.org/10.1021/acs.jpca.5c05841
J. Phys. Chem. A 2025, 129, 11032−11040

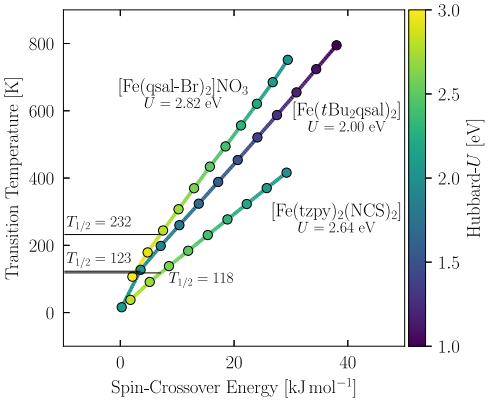

Figure 1. Variation of the transition temperature, $T_{1/2}$, and spin-crossover energy, ΔE_{sco}, as a function of the magnitude for the Hubbard-U correction. Results for the solid-state phases for the [Fe(tBu$_2$qsal)$_2$], [Fe(qsal-Br)$_2$]NO$_3$, and [Fe(tzpy)$_2$(NCS)$_2$] metal complexes are shown for comparison. The structures were taken from refs 75−77, whereas the data for [Fe(qsal-Br)$_2$]NO$_3$ and [Fe(tzpy)$_2$(NCS)$_2$] was obtained from ref 78.

metal complexes depicted therein, and then computing the phonons to get an estimate for $T_{1/2}$ and ΔE_{sco}. The details regarding these calculations follow later in the text. Arguably, fitting the Hubbard-U partially compensates the omitted long-range dispersion corrections, whereas including these weak interactions results in a slightly different calibrated U. The reason results from the fact that the Hubbard-U also adds a correction to the computed gradients during a geometry relaxation.

A related note regarding the use of Hubbard-U corrections is pertinent before proceeding. The magnitude of U is not universal and varies for different metal complexes regardless the oxidation state of the metallic core, as illustrated in Figure 1 for [Fe(tBu$_2$qsal)$_2$], [Fe(qsal-Br)$_2$]NO$_3$ with $T_{1/2}^{expt}$ = 232 K,[77] and [Fe(tzpy)$_2$(NCS)$_2$] with $T_{1/2}^{expt}$ = 118 K,[76] with ligands tBu$_2$qsal = 2,4-di(*tert*-butyl)-6-((quinoline-8-ylimino)methyl)-phenol, qsal-Br = (N-8-quino-lyl)-5-Br-salicylaldiminate, and tzpy = (3-(2-pyridyl)(1,2,3)triazolo(1,5-a)pyridine). The Hubbard-U magnitude is not transferable to a different choice of projector augmented wave potential.[88] Nor does U remain unchanged for distinct computational settings and methods, such as choice − Gaussian type orbitals or plane waves − and size of the basis set, electronic structure code, exchange-correlation density functional approximation, etc. In general, changes to the computational choices inevitably will result in a different U.

Having clarified the nuances surrounding the use of Hubbard-U corrections, we resume the description of the rest of the computational details. The plane wave kinetic energy cutoff was set to 600 eV, with augmentation charges evaluated with an auxiliary support grid. Nonspherical corrections to the electron density gradient also were included. The threshold for the convergence of the self-consistent field was set to 10^{-9} eV, with a Gaussian smearing width of 10^{-2} eV. Furthermore, because of the well-known spin−lattice coupling in spin-crossover materials, and in an effort to preserve as closely as possible the small variations in the crystal field strength during the spin conversion, the cell shape, its volume, and the atomic coordinates for all the solid-state materials discussed in this work were optimized with the conjugate gradient algorithm until forces were smaller than 10^{-3} eV Å^{-1}. The initial coordinates were obtained from the reported experimental structures. A k-point density of 0.2 Å^{-1} was used for this purpose, whereas solely the Gamma q-point was considered for phonon computations. These were done with a finite differences approach and a step size of 10^{-2} Å. Only the atoms through the first coordination shell for each of the Fe(II) centers in the unit cell were considered for the vibrational degrees of freedom.[78,89] The reasoning behind this choice is 2-fold, first due to the interest in developing methodologies that enable high-throughput treatment of large scale calculations, and second, as reported in ref 78, the contributions to the Gibbs free energy from the frequency-dependent terms in eqs 9 and 10 may be partially neglected as one moves away from the core of a metal complex. The basis for this assumption is the near cancellation between differences in the phonons from the low- and high-spin states that results in a strategic reduction of the number of degrees of freedom. The set of methodological choices, however, ultimately is an individual decision that relies upon the number of calculations, time, and the computing resources available for running the electronic structure calculations.

Furthermore, a series of representative configuration choices sampling the interval $0.0 \le n_{HS} \le 1.0$ in steps $\Delta n_{HS} = 1/4$ were used to compute an approximation to the phenomenological interaction parameter Γ in eq 17. For each unit cell, the generic labels L and H depict a metal center in a low- or high-spin state, respectively. As a result $n_{HS} = 0.0 \in \{LLLL\}$, $n_{HS} = 0.25 \in \{LLLH\}$, $n_{HS} = 0.5 \in \{LHLH, HLHL\}$, $n_{HS} = 0.75 \in \{HHHL\}$, and $n_{HS} = 1.0 \in \{HHHH\}$. The cell shape and volume, and the atomic coordinates were optimized for each configuration, followed by the phonon calculation. Both these steps were done using the methodology described in the previous paragraphs. Lastly, the least-squares fitting to eq 17 using all six spin configurations was performed with the pySCO library.

Treatment of all the output files and thermodynamic analyses were done with the pySCO library. In addition, the thermal variation of the magnetic susceptibility obtained from the pySCO output was approximated by

$$\mu_{S,L} = \sqrt{4S(S+1) + L(L+1)}\,\mu_B \tag{18}$$

where S and L are the total spin and spin momentum, respectively, and μ_B = 9.274 J T^{-1} is the Bohr magneton. $\mu_{S,L}$ is then expressed as an ensemble average for the low- and high-spin states weighted by n_{HS}.[90]

RESULTS AND DISCUSSION

Discussion of the results for the [Fe(tBu$_2$qsal)$_2$] metal complex evidently must start with the key contribution to $T_{1/2}$ in eq 6, namely, ΔE_{HL} as defined in eq 1, or ΔE_{sco} that includes the zero-point energy correction. As stated already, both quantities are readily available with pySCO. We obtained a ΔE_{HL} = 9.83 kJ mol^{-1}, that typically is reported in the field of materials science, or ΔE_{sco} = 3.21 kJ mol^{-1}, that instead commonly is preferred in quantum chemistry. Both values are well within the expected energy range for spin-switching materials. Though the calculated $T_{1/2}$ = 132 K is nine units larger than the average experimental reference, the calculated value is close to the upper experimental limit $T_{1/2}$ = 123 ± 6 K. In the absence of reliable confidence limits on the calculated values, de facto this amounts to agreement with experiment.

https://doi.org/10.1021/acs.jpca.5c05841
J. Phys. Chem. A 2025, 129, 11032−11040

With the $T_{1/2}$ validated, we proceed with the analysis of the thermal variation of the magnetic susceptibility, χT, by solving numerically the magnetization n_{HS} from eq 17 for $50 \leq T \leq 250$ K, which is handled automatically by pySCO, and then using eq 18 to convert the magnetization into χT. See ref 90 for details. For that it is necessary to compute the interaction parameter in eq 17 to model the hysteresis. In the interest of preserving a representative illustration, we considered a subset of six spin distributions that includes the pure low- and high-spin configurations, with $n_{HS} = 0$ and $n_{HS} = 1$, respectively, one for $n_{HS} = 1/4$, two configurations for $n_{HS} = 1/2$, and one for $n_{HS} = 3/4$. Their associated labels are LLLL, LLLH, LHLH, HLHL, HHHL, and HHHH, with L and H representing a metal center in a low- or high-spin state, respectively, in the unit cell. The computed ΔH for LLLH, LHLH, HLHL, and HHHL are 2.0, 8.22, 6.59, and 8.74 kJ mol^{-1}, respectively, where it is clear that the spin configuration HLHL energetically is more favorable than its counterpart LHLH by 1.63 kJ mol^{-1}, whereas HHHL follows closely the latter by 0.52 kJ mol^{-1}

The interaction parameter calculated via least-squares fitting is $\Gamma = 2.28$ kJ mol^{-1} with an $R^2 = 0.83$ that, in principle, can be improved by increasing the number of spin configurations for the fitting. That is beyond the scope of the present work. However, that Γ value yields no hysteresis. Details follow later in the discussion. As an aside, one may resort to fitting $\Gamma = 4$ kJ mol^{-1} that reproduces the experimental hysteresis width. Results in Figure 2 show the agreement between the computed

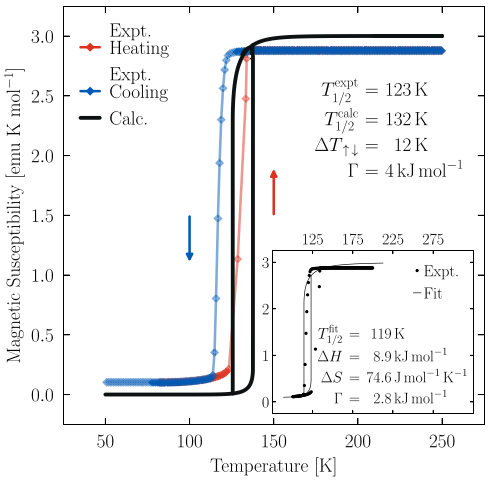

Figure 2. Comparison between the calculated and experimental transition temperature, $T_{1/2}$, and the temperature dependence of the magnetic susceptibility, χT, for $[Fe(tBu_2qsal)_2]$. The phenomenological interaction parameter, Γ, was fitted to reproduce the experimental hysteresis $\Delta T_{\uparrow\downarrow} = 12$ K. On the other hand, the reference quantities reported in the inset correspond to the Slichter and Drickamer model fitted with the experimental data for χT taken from ref 75. The number of points shown in the inset was reduced to ease visualization.

magnetic susceptibility with the experimental reference. A shifted spin transition is observed due to the 9 K overestimation for the calculated $T_{1/2}$ that leads to $\Delta H = 12.17$ kJ mol^{-1} and $\Delta S = 92.0$ J mol^{-1} K^{-1}. For comparison, the inset in Figure 2 shows the reference values $\Delta H = 8.9$ kJ mol^{-1}, $\Delta S = 74.6$ J mol^{-1} K^{-1}, and $\Gamma = 2.8$ kJ mol^{-1} that were extracted by fitting eq 17 to the experimental data. Both the predicted ΔH and ΔS agree reasonably well with the experiment, and eq 6 provides the basis to argue that the slight overestimation arises from the larger $T_{1/2}$ computed for the metal complex.

Details regarding the effects arising from the phenomenological interaction parameter, on the other hand, are better illustrated by monitoring the Gibbs free energy during the spin transition for the metal complex. The spin conversion may be classified into three regimes depending on the sign of the second derivative of eq 16 around $T_{1/2}$

$$\left(\frac{\partial^2 G}{\partial n_{HS}^2}\right)_{T,P,n_{HS}=1/2} = -2\Gamma + 4k_B N_A T_{1/2} \tag{19}$$

First are the weak interactions with $\partial^2 G/\partial n_{HS}^2 > 0$ that result in gradual spin conversions if $\Gamma < 2\ k_B N_A\ T_{1/2}$. It is the set of convex curves in Figure 3(a). Next is the critical point for which $\partial^2 G/\partial n_{HS}^2 = 0$ with abrupt transitions if $\Gamma = 2k_B N_A T_{1/2}$. It is highlighted in Figure 3(a) with the dotted line. This critical interaction for $[Fe(tBu_2qsal)_2]$ is 2.2 kJ mol^{-1}, close in magnitude to $\Gamma = 2.8$ kJ mol^{-1} calculated previously and thus the reason for the absence of hysteresis with the latter. Then come the strong interactions with $\partial^2 G/\partial n_{HS}^2 > 0$. It is the set of concave curves shown in Figure 3(a). Often this case involves first-order phase transitions and hysteresis,[8,91] with cooling $T_{\downarrow}$, transition $T_{1/2}$, and heating $T_{\uparrow}$ temperatures, each with an associated Gibbs free energy minimum, G_{min}, as shown in Figure 3(b). The possibility of observing three n_{HS} values for a $T_{\downarrow} \leq T \leq T_{\uparrow}$ is well established for this regime.[13] These may be related to stable, metastable or unstable spin configurations. See refs 92 and 65 for detailed discussions.

A more detailed analysis of the hysteresis regime, $T_{1/2} \pm 6$ K, for $[Fe(tBu_2qsal)_2]$ can be done by means of a series of isotherms for $-(\partial^2 G/\partial n_{HS}^2)_{T,P}$, as depicted in Figure 3(c). The negative Gibbs curvature shows favorable minima near $n_{HS} = 0$ and unfavorable near $n_{HS} = 1$ for $T < T_{\downarrow}$. The converse is observed for $T > T_{\uparrow}$. This is the typical behavior during spin conversion, namely, low temperatures favor the low-spin state, whereas high temperatures favor the high-spin state. For the hysteresis temperature interval, $T_{\downarrow} \leq T \leq T_{\uparrow}$, on the other hand, the existence of two minima is evident in Figure 3(c). In further detail, notice that there are metastable high-spin states near $n_{HS} = 0$ for $T_{\downarrow} \leq T < T_{1/2}$, whereas the presence metastable low-spin states near $n_{HS} = 1$ is observed for $T_{1/2} < T \leq T_{\uparrow}$. At the transition temperature, $T_{1/2}$, we can see in Figure 3(c) that there are two equally favorable minima near both $n_{HS} = 0$ and $n_{HS} = 1$. These minima are blocked energetically in the hysteresis temperature regime and, as a result, the metal complex may remain partially trapped in either spin state. A relatively slow relaxation toward the more stable spin state depends upon a delicate balance between temperature and the energy barrier height.

Lastly, it is worth noting that the experimental interaction parameter $\Gamma = 2.8$ kJ mol^{-1} for $[Fe(tBu_2qsal)_2]$ is close in magnitude to the 1.97, 2.30, and 2.97 kJ mol^{-1} reported[93] for $[Fe(btz)_2(NCS)_2]$,[94] $[Fe(bpz)_2(bipy)_2]$,[95] and $[Fe(phen)_2(NCS)_2]$,[96] respectively, with ligands phen = 1,2-phenanthroline, btz = 5,5′,6,6′-tetrahydro-4*H*,4′*H*-2-2′-bi-1,3-thiazine, dpz = dihydrobis(1-pyrazolil)borate, and bipy = 2,2′-bipyridine. All these metal complexes share somewhat similar asymmetric steric hindrance and are considered attractive for use in sublimation techniques to fabricate thin films,[9] which confirms the importance of understanding the influence of different choices of ligands upon the intermolecular interactions for these materials.

https://doi.org/10.1021/acs.jpca.5c05841
J. Phys. Chem. A 2025, 129, 11032−11040

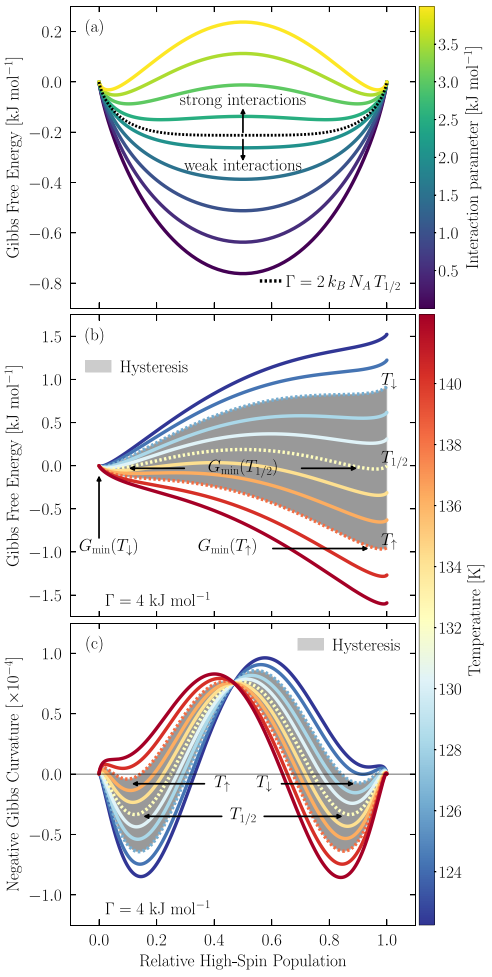

Figure 3. (a) Isothermal Gibbs free energy, G, for the progressively increasing relative high-spin population, n_{HS}, for different choices of the phenomenological interaction parameter, Γ. The critical point $\Gamma = 2k_BN_AT_{1/2}$ delimits the region between weakly and strongly interacting molecules. All the isotherms are for the computed transition temperature $T_{1/2}$ = 132 K. (b) Gibbs free energy as a function of the relative high-spin population for different choices of temperature at fixed Γ = 4 kJ mol^{-1}. Three isotherms are highlighted, namely, $T_\downarrow$, $T_{1/2}$, and $T_\uparrow$, that correspond to the cooling, transition, and heating temperature, respectively. (c) $-(\partial^2 G/\partial n_{HS}^2)_{T,P}$ for various temperatures. The shaded area in panels (b) and (c) depicts the hysteresis temperature interval $T_\downarrow \le T \le T_\uparrow$, whereas the dotted lines depict the cooling, transition, and heating temperature $T_\downarrow$, $T_{1/2}$, and $T_\uparrow$, respectively.

CONCLUDING REMARKS

In summary, this work showed that the pySCO library allows for conducting high-throughput scalable analyses with greater ease, facilitating the study of the spin conversion phenomenon in molecules and solid state materials. By showcasing its use on the $[Fe(tBu_2qsal)_2]$ metal complex, the influence of the phenomenological interaction parameter was discussed using the mean field regular solution model available in the library. The results serve to provide a detailed examination of the interaction regimes for this complex. These are in part responsible for the volatility characteristics in asymmetric metal complexes, which are of interest for the preparation of ultrathin interface heterostructures.

ASSOCIATED CONTENT

Data Availability Statement

The pySCO library is an open source project and is available for download in the public repository github.com/amalbavera/pysco. The library uses the International System of Units, therefore, the spin conversion energy ΔE_{sco}, the enthalpy ΔH, and the phenomenological interaction parameter Γ are in kJ mol^{-1}, whereas the temperature T is in Kelvin, and the entropy ΔS in J mol^{-1} K^{-1}. The repository also collects the VASP output files for the $[Fe(tBu_2qsal)_2]$ metal complex needed for the calculation of the spin crossover energy, transition temperature, and analyses for the phenomenological interaction parameter. A Jupyter notebook also is included with illustrative code blocks to reproduce the results.

AUTHOR INFORMATION

Corresponding Author

Angel Albavera-Mata − *Department of Physics, University of Florida, Gainesville, Florida 32611, United States; Center for Molecular Magnetic Quantum Materials, Gainesville, Florida 32611, United States;* orcid.org/0000-0003-1521-678X; Email: aalbaveramata@ufl.edu

Complete contact information is available at: https://pubs.acs.org/10.1021/acs.jpca.5c05841

Notes

The author declares no competing financial interest.

ACKNOWLEDGMENTS

The author is grateful to S.B. Trickey, Richard G. Hennig, and Xiao-Guang Zhang for constructive discussions and their insightful remarks. This work was supported as part of the Center for Molecular Magnetic Quantum Materials, an Energy Frontier Research Center funded by the U.S. Department of Energy, Office of Science, Basic Energy Sciences under Award No. DE-SC0019330. This research used resources of the National Energy Research Scientific Computing Center (NERSC), a Department of Energy Office of Science User Facility using NERSC award BES-ERCAP0022828.

ACRONYMS

LS	low-spin
HS	high-spin
PBE	Perdew−Burke−Ernzerhof
VASP	Vienna Ab initio Simulation Package

REFERENCES

(1) Gütlich, P.; Ksenofontov, V.; Gaspar, A. B. Pressure effect studies on spin crossover systems. *Coord. Chem. Rev.* **2005**, *249*, 1811−1829.

(2) Bousseksou, A.; Molnár, G.; Salmona, L.; Nicolazzi, W. Molecular spin crossover phenomenon: recent achievements and prospects. *Chem. Soc. Rev.* **2011**, *40*, 3313−3335.

(3) Gaspar, A. B.; Seredyuk, M. Spin crossover in soft matter. *Coord. Chem. Rev.* **2014**, *268*, 41−58.

(4) Hogue, R. W.; Singh, S.; Brooker, S. Spin crossover in discrete polynuclear iron(II) complexes. *Chem. Soc. Rev.* **2018**, *47*, 7303−7338.

(5) Brady, C.; McGarvey, J. J.; McCusker, J. K.; Toftlund, H.; Hendrickson, D. N. Time-Resolved Relaxation Studies of Spin Crossover Systems in Solution. *Top. Curr. Chem.* **2004**, *235*, 1−22.

(6) Rodríguez-Jiménez, S.; Brooker, S. Solid Versus Solution Spin Crossover and the Importance of the Fe-N≡C(X) Angle. *Inorg. Chem.* **2017**, *56*, 13697−13708.
(7) Wang, J.; Li, Y.; Wei, R.-J.; Tang, Z.; Yao, Z.-S.; Tao, J. Spin-Crossover Behaviors of Iron(II) Complexes Bearing Halogen Ligands in Solid State and Solution. *Inorg. Chem.* **2023**, *62*, 1354−1361.
(8) Ridier, K.; Molnár, G.; Salmon, L.; Nicolazzi, W.; Bousseksou, A. Hysteresis, nucleation and growth phenomena in spin-crossover solids. *Solid State Sci.* **2017**, *74*, A1−A22.
(9) Kumar, K. S.; Ruben, M. Sublimable Spin-Crossover Complexes: From Spin-State Switching to Molecular Devices. *Angew. Chem., Int. Ed.* **2021**, *60*, 7502−7521.
(10) Kipgen, L.; Bernien, M.; Tuczek, F.; Kuch, W. Spin-Crossover Molecules on Surfaces: From Isolated Molecules to Ultrathin Films. *Adv. Mater.* **2021**, *33*, 2008141.
(11) Amin, N. A. A. M.; Said, S. M.; Salleh, M. F. M.; Afifi, A. M.; Ibrahim, N. M. J. N.; Hasnan, M. M. I. M.; Tahir, M.; Hashim, N. Review of Fe-based spin crossover metal complexes in multiscale device architectures. *Inorg. Chim. Acta* **2023**, *544*, 121168.
(12) Yazdani, S.; Phillips, J.; Ekanayaka, T. K.; Cheng, R.; Dowben, P. A. The Influence of the Substrate on the Functionality of Spin Crossover Molecular Materials. *Molecules* **2023**, *28*, 3735.
(13) Kahn, O. *Molecular Magnetism*; VCH Publishers Inc: New York, 1993.
(14) Jean, Y. *Molecular Orbitals of Transition Metal Complexes*; Oxford University Press: New York, 2005.
(15) Mohn, P. *Magnetism in the Solid State*; Springer-Verlag: Berlin Heidelberg, 2006.
(16) Dimian, M.; Rotaru, A. *Magnetic Materials*; Maaz, K., Ed.; IntechOpen: Rijeka, 2016, Chapter 5.
(17) Hauser, A. In *Spin crossover in transition metal compounds*; Gütlich, P.; Goodwin, H. A., Eds.; Springer: Berlin: New York, 2004; pp 49−58.
(18) Gütlich, P.; Goodwin, H. A. *Spin crossover in transition metal compounds I*; Gütlich, I.; Goodwin, P., Eds.; Springer: Berlin: Heidelberg, 2004; pp 1−47.
(19) Y Garcia, P. G. *Spin Crossover in Transition Metal Compounds II*; Gütlich, P.; Goodwin, H. A., Eds.; Springer: Berlin: Heidelberg, 2004; pp 49−62.
(20) Létard, J.-F.; Guionneau, P.; Goux-Capes, L. *Spin Crossover in Transition Metal Compounds III*; Gütlich, P.; Goodwin, H. A., Eds.; Springer: Berlin: Heidelberg, 2004; pp 221−249.
(21) Polanyi, M. Colloquium im Kaiser Wilhelm-Institut für physikalische Chemie und Elektrochemie. *Angew. Chem.* **1931**, *44*, 207−208.
(22) Cambi, L.; Szegö, L. Über die magnetische Susceptibilität der komplexen Verbindungen. *Ber. Dtsch. Chem. Ges.* **1931**, *64*, 2591−2598.
(23) Baker, W. A.; Bobonich, H. M. Magnetic Properties of Some High-Spin Complexes of Iron(II). *Inorg. Chem.* **1964**, *3*, 1184−1188.
(24) König, E.; Madeja, K. Unusual magnetic behaviour of some iron(II)−bis-(1,10-phenanthroline) complexes. *Chem. Commun.* **1966**, *1966*, 61−62.
(25) Wajnflasz, J. Etude de la transition "Low Spin"-"High Spin" dans les complexes octaédriques d'ion de transition. *Phys. Status Solidi* **1970**, *40*, 537−545.
(26) Wajnflasz, J.; Pick, R. Transitions Low Spin - High Spin dans les Complexes de Fe^{2+}. *J. Phys. Colloq.* **1971**, *32*, 90−91.
(27) Boča, R.; Linert, W. Is There a Need for New Models of the Spin Crossover? *Montash. Chem.* **2003**, *134*, 199−216.
(28) Koudriavtsev, A. B.; Linert, W. Spin Crossover − an Unusual Chemical Equilibrium. *J. Struct. Chem.* **2010**, *51*, 335−365.
(29) Pavlik, J.; Boča, R. Established Static Models of Spin Crossover. *Eur. J. Inorg. Chem.* **2013**, *2013*, 697−709.
(30) Gaspar, A. B.; Ksenofontov, V.; Seredyuk, M.; Gütlich, P. Multifunctionality in spin crossover materials. *Coord. Chem. Rev.* **2005**, *249*, 2661−2667.
(31) Gaspar, A. B.; Seredyuk, M.; Gütlich, P. Spin crossover in metallomesogens. *Coord. Chem. Rev.* **2009**, *253*, 2399−2413.
(32) Gaspar, A. B.; Seredyuk, M.; Gütlich, P. Spin crossover in iron(II) complexes: Recent advances. *J. Mol. Struct.* **2009**, *924−926*, 9−19.
(33) Atmani, C.; Hajj, F. E.; Benmansour, S.; Marchivie, M.; Triki, S.; Conan, F.; Patinec, V.; Handel, H.; Dupouy, G.; Gómez-García, C. J. Guidelines to design new spin crossover materials. *Coord. Chem. Rev.* **2010**, *254*, 1559−1569.
(34) Harding, D. J.; Harding, P.; Phonsri, W. Spin crossover in iron(III) complexes. *Coord. Chem. Rev.* **2016**, *313*, 38−61.
(35) Ferrando-Soria, J.; Vallejo, J.; Castellano, M.; Martínez-Lillo, J.; Pardo, E.; Cano, J.; Castro, I.; Lloret, F.; Ruiz-Garcia, R.; Julve, M. Molecular magnetism, quo vadis? A historical perspective from a coordination chemist viewpoint. *Coord. Chem. Rev.* **2017**, *339*, 17−103.
(36) Wang, M.; Li, Z.-Y.; Ishikawa, R.; Yamashita, M. Spin crossover and valence tautomerism conductors. *Coord. Chem. Rev.* **2021**, *435*, 213819.
(37) Tao, J.; Wei, R.-J.; Huang, R.-B.; Zheng, L.-S. Polymorphism in spin-crossover systems. *Chem. Soc. Rev.* **2012**, *41*, 703−737.
(38) Collet, E.; Guionneau, P. Structural analysis of spin-crossover materials: From molecules to materials. *Comptes Rendus Chimie* **2018**, *21*, 1133−1151.
(39) Matouzenko, G. S.; Bousseksou, A.; Lecocq, S.; van Koningsbruggen, P. J.; Perrin, M.; Kahn, O.; Collet, A. Polymorphism in Spin Transition Systems. Crystal Structure, Magnetic Properties, and Mo1 ssbauer Spectroscopy of Three Polymorphic Modifications of [Fe(DPPA)(NCS)2] [DPPA= (3-Aminopropyl)bis(2-pyridylmethyl)amine]. *Inorg. Chem.* **1997**, *36*, 5869−5879.
(40) Frisch, M. J.; Trucks, G. W.; Schlegel, H. B.; Scuseria, G. E.; Robb, M. A.; Cheeseman, J. R.; Scalmani, G.; Barone, V.; Petersson, G. A.; Nakatsuji, H.et al. *Gaussian*; Gaussian Inc: Wallingford CT, 2016.
(41) Valiev, M.; Bylaska, E. J.; Govind, N.; Kowalski, K.; Straatsma, T.; Van Dam, H.; Wang, D.; Nieplocha, J.; Apra, E.; Windus, T.; de Jong, W. NWChem: A comprehensive and scalable open-source solution for large scale molecular simulations. *Comput. Phys. Commun.* **2010**, *181*, 1477.
(42) Neese, F. Software update: The ORCA program system—Version 5.0. *WIRES Comput. Mol. Sci.* **2022**, *12*, e1606.
(43) Kresse, G.; Furthmüller, J. Efficient Iterative Schemes for Ab Initio Total-Energy Calculations Using a Plane-Wave Basis Set. *Phys. Rev. B* **1996**, *54*, 11169.
(44) Giannozzi, P.; Andreussi, O.; Brumme, T.; Bunau, O.; Buongiorno Nardelli, M.; Calandra, M.; Car, R.; Cavazzoni, C.; Ceresoli, D.; Cococcioni, M.; et al. Advanced capabilities for materials modelling with QUANTUM ESPRESSO. *J. Phys.: Condens. Matter* **2017**, *29*, 465901.
(45) König, E.Nature and dynamics of the spin-state interconversion in metal complexes. In *Structure and Bonding* 1991; Vol. *76*, pp 51−152.
(46) Bousseksou, A.; Nasser, J.; Linares, J.; Boukheddaden, K.; Varret, F. Ising-like model for the two-step spin-crossover. *J. Phys. I France* **1992**, *2*, 1381−1403.
(47) Bousseksou, A.; Varret, F.; Nasser, J. Ising-like model for the two step spin-crossover of binuclear molecules. *J. Phys. I France* **1993**, *3*, 1463−1473.
(48) Linares, J.; Nasser, J.; Bousseksou, A.; Boukheddaden, K.; Varret, F. Monte Carlo simulations of spin-crossover transitions using the two-level model. I: Mononuclear single sublattice case. *J. Mag. Mag. Mater.* **1995**, *140−144*, 1503−1504.
(49) Linares, J.; Nasser, J.; Bousseksou, A.; Boukheddaden, K.; Varret, F. Monte Carlo simulations of spin-crossover transitions using the two level model. II: Binuclear case. *J. Mag. Mag. Mater.* **1995**, *140−144*, 1507−1508.
(50) Stoleriu, L.; Chakraborty, P.; Hauser, A.; Stancu, A.; Enachescu, C. Thermal hysteresis in spin-crossover compounds studied within the mechanoelastic model and its potential application to nanoparticles. *Phys. Rev. B* **2011**, *84*, 134102.

https://doi.org/10.1021/acs.jpca.5c05841
J. Phys. Chem. A 2025, 129, 11032−11040

(51) Pavlik, J.; Nicolazzi, J. P. W.; Nicolazzi, W.; Molnár, G.; Molnár, G.; Boča, R.; Boča, R.; Bousseksou, A. Coupled magnetic interactions and the Ising-like model for spin crossover in binuclear compounds. *Eur. Phys. J. B* **2013**, *86*, 292.
(52) Mikolasek, M.; Nicolazzi, W.; Terki, F.; Molnár, G.; Bousseksou, A. Investigation of surface energies in spin crossover nanomaterials: the role of surface relaxations. *Phys. Chem. Chem. Phys.* **2017**, *19*, 12276−12281.
(53) Markin, O.; Gudyma, I.; Boukheddaden, K. Role of harmonic and anharmonic interactions in controlling the cooperativity of spin-crossover molecular crystals. *Phys. Rev. B* **2024**, *110*, 174416.
(54) Hildebrand, J. H.; Scott, R. L. *Regular Solutions*; Prentice-Hall International Series in ChemistryPrentice-Hall, 1962.
(55) Hildebrand, J. H.; Prausnitz, J. M.; Scott, R. L. *Regular and Related Solutions: the Solubility of Gases, Liquids, and Solids*; Van Nostrand Reinhold Co.: New York, 1970.
(56) McQuarrie, D. A. *Statistical Mechanics*; Harper and Row: New York, 1976; pp 35−64.
(57) McQuarrie, D. A.; Simon, J. D. *Molecular Thermodynamics*; University Science Books: Sausalito CA, 1999; pp 143−168.
(58) Quintano, M. M.; Silva, M. X.; Belchior, J. C.; Braga, J. P. Electronic Entropy as a Periodic Property of the Elements: A Theoretical Chemistry Approach. *J. Chem. Educ.* **2021**, *98*, 2574−2577.
(59) Nicholson, D. M. C.; Stocks, G. M.; Wang, Y.; Shelton, W. A.; Szotek, Z.; Temmerman, W. M. Stationary nature of the density-functional free energy: Application to accelerated multiple-scattering calculations. *Phys. Rev. B* **1994**, *50*, 14686R.
(60) Slichter, C. P.; Drickamer, H. G. Pressure-Induced Electronic Changes in Compounds of Iron. *J. Chem. Phys.* **1972**, *56*, 2142−2160.
(61) Boukheddaden, K.; Shteto, I.; Hôo, B.; Varret, F. Dynamical model for spin-crossover solids. I. Relaxation effects in the mean-field approach. *Phys. Rev. B* **2000**, *62*, 14796.
(62) Boukheddaden, K.; Shteto, I.; Hôo, B.; Varret, F. Dynamical model for spin-crossover solids. II. Static and dynamic effects of light in the mean-field approach. *Phys. Rev. B* **2000**, *62*, 14806.
(63) Kepenekian, M.; Guennic, B. L.; Robert, V. Magnetic bistability: From microscopic to macroscopic understandings of hysteretic behavior using ab initio calculations. *Phys. Rev. B* **2009**, *79*, 094428.
(64) Enachescu, C.; Nicolazzi, W. Elastic models, lattice dynamics and finite size effects in molecular spin crossover systems. *Comptes Rendus. Chimie* **2018**, *21*, 1179−1195.
(65) Nicolazzi, W.; Bousseksou, A. Thermodynamical aspects of the spin crossover phenomenon. *C. R. Chimie* **2018**, *21*, 1060−1074.
(66) Collet, E.; Azzolina, G. Coupling and decoupling of spin crossover and ferroelastic distortion: Unsymmetric hysteresis loop, phase diagram, and sequence of phases. *Phys. Rev. Mater.* **2021**, *5*, 044401.
(67) Tchougrkeff, A. L. Lattice Relaxation and Cooperativity in the Low-Spin to High-Spin Transitions in Molecular Crystals. *Mol. Cryst. Liq. Cryst. Sci. Technol., Sect. A* **1995**, *274*, 17−23.
(68) Tchougréeff, A. L.; Darkhovskii, M. B. Lattice relaxation and order in the low-spin to high-spin transitions in molecular crystals. *Int. J. Quantum Chem.* **1996**, *57*, 903−912.
(69) Paulsen, H. Periodic Density Functional Calculations in Order to Assess the Cooperativity of the Spin Transition in Fe-$(phen)_2(NCS)_2$. *Magnetochemistry* **2016**, *2*, 14.
(70) De, S.; Tewary, S.; Garnier, D.; Li, Y.; Gontard, G.; Lisnard, L.; Flambard, A.; Breher, F.; Boillot, M.-L.; Rajaraman, G.; Lescouëzec, R. Solution and Solid-State Study of the Spin-Crossover $[Fe^{II}(R\text{-}bik)_3](BF4)_2$ Complexes (R = Me, Et, Vinyl). *Aur. J. Inorg. Chem.* **2018**, *2018*, 208−543.
(71) Vela, S.; Paulsen, H. Cooperativity in Spin Crossover Systems. An Atomistic Perspective on the Devil's Staircase. *Inorg. Chem.* **2018**, *57*, 9478−9488.
(72) Pillet, S. Spin-crossover materials: Getting the most from x-ray crystallography. *J. Appl. Phys.* **2021**, *129*, 181101.
(73) Popa, A.-I.; Stoleriu, L.; Enachescu, C. Tutorial on the elastic theory of spin crossover materials. *J. Appl. Phys.* **2021**, *129*, 131101.
(74) Wolny, J. A.; Gröpl, K.; Kiehl, J.; Rentschler, E.; Schünemann, V. Quantification of the thermodynamic effects of the low-spin − high-spin interaction in molecular crystals of a mononuclear iron(ii) spin crossover complex. *Dalton Trans.* **2024**, *53*, 8391−8397.
(75) Gakiya-Teruya, M.; Jiang, X.; Le, D.; Üngör, Ö.; Durrani, A. J.; Koptur-Palenchar, J. J.; Jiang, J.; Jiang, T.; Meisel, M. W.; Cheng, H.-P.; Zhang, X.-G.; Zhang, X.-X.; Rahman, T. S.; Hebard, A. F.; Shatruk, M. Asymmetric Design of Spin-Crossover Complexes to Increase the Volatility for Surface Deposition. *J. Am. Chem. Soc.* **2021**, *143*, 14563−14572.
(76) Niel, V.; Gaspar, A. B.; Muñoz, M. C.; Abarca, B.; Ballesteros, R.; Real, J. A. Spin Crossover Behavior in the Iron(II)-2-pyridyl-[1,2,3]triazolo[1,5-a]pyridine System: X-ray Structure, Calorimetric, Magnetic, and Photomagnetic Studies. *Inorg. Chem.* **2003**, *42*, 4782−4788.
(77) Harding, D. J.; Phonsri, W.; Harding, P.; Murray, K. S.; Moubaraki, B.; Jameson, G. N. L. Abrupt two-step and symmetry breaking spin crossover in an iron(iii) complex: an exceptionally wide [LS−HS] plateau. *Dalton Trans.* **2015**, *44*, 15079−15082.
(78) Albavera-Mata, A.; Hennig, R. G.; Trickey, S.B. Transition Temperature for Spin-Crossover Materials with the Mean Value Ensemble Hubbard-U Correction. *J. Phys. Chem. A* **2023**, *127*, 7646−7654.
(79) Radoń, M. Revisiting the role of exact exchange in DFT spin-state energetics of transition metal complexes. *Phys. Chem. Chem. Phys.* **2014**, *16*, 14479−14488.
(80) Kepp, K. P. Theoretical Study of Spin Crossover in 30 Iron Complexes. *Inorg. Chem.* **2016**, *55*, 2717−2727.
(81) Kepp, K. P. *Transition Metals in Coordination Environments: Computational Chemistry and Catalysis Viewpoints*; Broclawik, E.; Borowski, T.; Radoń, M., Eds.; Springer International Publishing: Cham, 2019; pp 1−33.
(82) Song, S.; Kim, M.-C.; Sim, E.; Benali, A.; Heinonen, O.; Burke, K. Benchmarks and Reliable DFT Results for Spin Gaps of Small Ligand Fe(II) Complexes. *J. Chem. Theory Comput.* **2018**, *14*, 2304−2311.
(83) Phung, Q. M.; Feldt, M.; Harvey, J. N.; Pierloot, K. Toward Highly Accurate Spin State Energetics in First-Row Transition Metal Complexes: A Combined CASPT2/CC Approach. *J. Chem. Thoery Comput.* **2018**, *14*, 2446−2455.
(84) Perdew, J. P.; Burke, K.; Ernzerhof, M. Generalized Gradient Approximation Made Simple. *Phys. Rev. Lett.* **1996**, *77*, 3865.
(85) Perdew, J. P.; Burke, K.; Ernzerhof, M. Generalized Gradient Approximation Made Simple [Phys. Rev. Lett. **77**, 3865 (1996)]. *Phys. Rev. Lett.* **1997**, *78*, 1396.
(86) Dudarev, S. L.; Botton, G. A.; Savrasov, S. Y.; et al. Electron-Energy-Loss Spectra and the Structural Stability of Nickel Oxide: An LSDA+U Study. *Phys. Rev. B* **1998**, *57*, 1505.
(87) Tolba, S. A.; Gameel, K. M.; Ali, B. A.; Almossalami, H. A.; Allam, N. K. *Density Functional Calculations*; Yang, G., Ed.; IntechOpen: Rijeka, 2018, Chapter 1.
(88) Albavera-Mata, A.; Hennig, R. G.; Trickey, S.B. Mean Value Ensemble Hubbard-U Correction for Spin-Crossover Molecules. *J. Phys. Chem. Lett.* **2022**, *13*, 12049−12054.
(89) Albavera-Mata, A.; Liu, S.; Cheng, H.-P.; Hennig, R. G.; Trickey, S.B. Magnetic and Thermodynamic Computations for Supramolecular Assemblies between a Cr(III) and Fe(III) Single-Ion Magnet and an Fe(II) Spin-Crossover Complex. *J. Phys. Chem. A* **2024**, *128*, 10929−10935.
(90) Mugiraneza, S.; Hallas, A. M. Tutorial: a beginner's guide to interpreting magnetic susceptibility data with the Curie-Weiss law. *Commun. Phys.* **2022**, *5*, 95.
(91) Halcrow, M. A. *Spin-Crossover Materials*; John Wiley & Sons, Ltd, 2013; Chapter 5, pp 147−169.
(92) Brooker, S. Spin crossover with thermal hysteresis: practicalities and lessons learnt. *Chem. Soc. Rev.* **2015**, *44*, 2880−2892.

https://doi.org/10.1021/acs.jpca.5c05841
J. Phys. Chem. A 2025, 129, 11032−11040

(93) Sinitskiy, A. V.; Tchougréeff, A. L.; Dronskowski, R. Phenomenological model of spin crossover in molecular crystals as derived from atom−atom potentials. *Phys. Chem. Chem. Phys.* **2011**, *13*, 13238−13246.
(94) Real, J. A.; Gallois, B.; Granier, T.; Suez-Panama, F.; Zarembowitch, J. Comparative investigation of the spin-crossover compounds $Fe(btz)_2(NCS)_2$ and $Fe(phen)_2(NCS)_2$ (where btz = 2,2′-bi-4,5-dihydrothiazine and phen = 1,10-phenanthroline). Magnetic properties and thermal dilatation behavior and crystal structure of $Fe(btz)_2(NCS)_2$ at 293 and 130 K. *Inorg. Chem.* **1992**, *31*, 4972−4979.
(95) Real, J. A.; Muñoz, M. C.; Faus, J.; Solans, X. Spin Crossover in Novel Dihydrobis(1-pyrazolyl)borate $[H_2B(pz)_2]$-Containing Iron(II) Complexes. Synthesis, X-ray Structure, and Magnetic Properties of $[FeL\{H_2B(pz)_2\}_2]$ (L = 1,10-Phenanthroline and 2,2′-Bipyridine). *Inorg. Chem.* **1997**, *36*, 3008−3013.
(96) Gallois, B.; Real, J.-A.; Hauw, C.; Zarembowitch, J. Structural changes associated with the spin transition in bis(isothiocyanato)bis(1,10-phenanthroline)iron: a single-crystal x-ray investigation. *Inorg. Chem.* **1990**, *29*, 1152−1158.

https://doi.org/10.1021/acs.jpca.5c05841
J. Phys. Chem. A 2025, 129, 11032−11040